

---

# RFWave: Multi-band Rectified Flow for Audio Waveform Reconstruction

---

**Peng Liu**  
laupeng1989@gmail.com

**Dongyang Dai**  
accum.dai@gmail.com

**Zhiyong Wu**  
Shenzhen International Graduate School, Tsinghua University  
zywu@sz.tsinghua.edu.cn

## Abstract

Recent advancements in generative modeling have significantly enhanced the reconstruction of audio waveforms from various representations. While diffusion models are adept at this task, they are hindered by latency issues due to their operation at the individual sample point level and the need for numerous sampling steps. In this study, we introduce RFWave, a cutting-edge multi-band Rectified Flow approach designed to reconstruct high-fidelity audio waveforms from Mel-spectrograms or discrete tokens. RFWave uniquely generates complex spectrograms and operates at the frame level, processing all subbands simultaneously to boost efficiency. Leveraging Rectified Flow, which targets a flat transport trajectory, RFWave achieves reconstruction with just 10 sampling steps. Our empirical evaluations show that RFWave not only provides outstanding reconstruction quality but also offers vastly superior computational efficiency, enabling audio generation at speeds up to 97 times faster than real-time on a GPU. An online demonstration is available at: <https://rfwave-demo.github.io/rfwave/>.

## 1 Introduction

Audio waveform reconstruction significantly enhances the digital interactions by enabling realistic voice and sound generation for diverse applications. This technology transforms low-dimensional features, derived from raw audio data, into perceptible sounds, improving the audio experience on various platforms such as virtual assistants and entertainment systems. The main challenges in this field focus on improving the quality of reconstructed audio and speeding up audio generation.

Prior to the widespread adoption of neural networks, audio waveform reconstruction methods such as STRAIGHT [1] and WORLD [2], based on speech signal processing techniques, were introduced. These methods reconstructed audio from low-dimensional features, delivering clear speech but sacrificing many details, rendering the output noticeably synthetic. However, deep learning has greatly enhanced audio waveform reconstruction models, evolving alongside neural network-based generative models.

Autoregressive models were first applied to the task of audio waveform reconstruction. WaveNet [3] notably advanced audio quality beyond prior signal processing methods, although it was hindered by slow generation speeds. Following this, WaveRNN [4] improved generation speed using a lightweight RNN and dual softmax layer. Furthermore, LPCNet [5] leveraged speech signal processing domain knowledge to reduce model complexity, enhancing both generation speed and audio clarity.

Nevertheless, the inherent slowness of autoregressive models, which generate sample points sequentially, sparked a demand for parallel generation. The rise of Generative Adversarial Networks (GAN)

[6] inspired new research directions in audio waveform reconstruction. MelGAN [7], for example, utilized Mel-spectrograms as inputs to generate all corresponding waveform sample points in parallel, achieving speeds hundreds of times faster than real-time on GPUs. Models like Parallel WaveGAN [8] and HiFi-GAN [9] further refined the model architecture and discriminators, enhancing the quality of generated audio. Due to their relatively good performance and rapid generation speeds, GAN-based models quickly became mainstream in the industry. Considering that speech signals consist of a large number of sample points per second, modeling speech waveforms typically incorporates upsampling layers. A notable advancement in this aspect is the replacement of certain upsampling layers with the Inverse Short-Time Fourier Transform (ISTFT) in models like iSTFTNET [10], APNet2 [11], and Vocos [12]. This substitution not only simplifies the network architecture but also enhances computational efficiency, resulting in faster processing speeds while maintaining the quality of the speech.

Despite their advancements, GAN-based waveform reconstruction models face challenges such as the need for intricate discriminator designs and issues like instability and mode collapse. In response to these challenges, diffusion models for waveform reconstruction have been explored. For example, Diffwave [13] outperforms both WaveNet and WaveGAN [14]. PriorGrad [15] improves both the quality of speech and the speed of inference through the use of a data-dependent prior distribution, while FreGrad [16] simplifies the model and reduces denoising time by using Discrete Wavelet Transform (DWT).

Recently, neural codecs have gained increasing attention. These codecs offer superior compression rates compared to traditional signal processing methods, showing significant potential for applications in communication and storage. Additionally, they are capable of converting audio into discrete tokens, facilitating the integration of audio data with other modalities during the modeling process, as demonstrated by VALL-E [17] and UniAudio [18]. Typically, these neural codecs employ GAN-based decoder for waveform reconstruction, as seen in SoundStream [19] and EnCodec [20]. However, the recent Multi-Band Diffusion (MBD) [21] utilizes a diffusion model, which significantly enhances the quality and detail of the reconstructed waveform.

Despite producing relatively high-quality audio, diffusion-based waveform reconstruction has not gained widespread industry adoption due to the substantial computational costs and noticeable latency associated with its requirement for multiple sampling steps. In this paper, we propose RFWave, using Rectified Flow [22] for waveform reconstruction. Its inference speed can reach up to 97 times real-time on an NVIDIA GeForce RTX 4090 GPU. To our knowledge, RFWave stands as the fastest diffusion-based audio waveform reconstruction model, and it delivers superior audio quality. To accomplish its superior generation performance and computational efficiency, our main contributions are as follows:

1. By integrating the Rectified Flow and 3 enhanced loss functions – energy-balanced loss, overlap loss, and Short-Time Fourier Transform (STFT) loss – our model can reconstruct high-quality waveforms with a drastically reduced number of sampling steps.
2. We utilize a multi-band strategy, coupled with the high-efficiency ConvNeXtV2 [23] backbone, to generate different subbands concurrently. This not only assures audio quality by circumventing cumulative errors, but also boosts the synthesis speed.
3. Our model operates at the level of STFT frames, not individual waveform sample points. This approach significantly accelerates processing and reduces GPU memory usage.

## 2 Background

In this section, we describe the basic formulation of the Rectified Flow and present related works, while also detailing our correlation and distinction.

**Rectified Flow** Rectified Flow [22] presents an innovative ODE-based framework for generative modeling and domain transfer. It introduces a method to learn a transport mapping that connects two distributions,  $\pi_0$  and  $\pi_1$  on  $\mathbb{R}^d$ , based on empirical observations:

$$\frac{dZ_t}{dt} = v(Z_t, t), \quad \text{initialized from } Z_0 \sim \pi_0, \text{ such that } Z_1 \sim \pi_1, \quad (1)$$

where  $v: \mathbb{R}^d \times [0, 1] \rightarrow \mathbb{R}^d$  represents a velocity field. The learning of this field involves minimizing a mean square objective function,

$$\min_v \mathbb{E}_{(X_0, X_1) \sim \gamma} \left[ \int_0^1 \left\| \frac{d}{dt} X_t - v(X_t, t) \right\|^2 dt \right], \quad \text{with } X_t = \phi(X_0, X_1, t), \quad (2)$$

where  $X_t = \phi(X_0, X_1, t)$  represents a time-differentiable interpolation between  $X_0$  and  $X_1$ , with  $\frac{d}{dt} X_t = \partial_t \phi(X_0, X_1, t)$ . The  $\gamma$  represents any coupling of  $(\pi_0, \pi_1)$ . An illustrative instance of  $\gamma$  is the independent coupling  $\gamma = \pi_0 \times \pi_1$ , which allows for empirical sampling based on separately observed data from  $\pi_0$  and  $\pi_1$ . The authors recommended a simple choice of

$$X_t = (1 - t)X_0 + tX_1 \implies \frac{d}{dt} X_t = X_1 - X_0. \quad (3)$$

This simplification results in linear trajectories, which are critical for accelerating the inference process. Typically, the velocity field  $v$  is represented using a deep neural network. The solution to (2) is approximated through stochastic gradient methods. To approximate the ODE presented in (1), numerical solvers are commonly employed. A prevalent technique is the forward Euler method. This approach computes values using the formula

$$Z_{t+\frac{1}{n}} = Z_t + \frac{1}{n} v(Z_t, t), \quad \forall t \in \{0, \dots, n-1\}/n, \quad (4)$$

where the simulation is executed with a step size of  $\epsilon = 1/n$  over  $n$  steps.

The velocity field has the capacity to incorporate conditional information, which is particularly essential in applications such as text-to-image generation and waveform reconstruction from Mel-spectrograms. Consequently, in such contexts,  $v(Z_t, t)$  in (2) is modified to  $v(Z_t, t | \mathcal{C})$ , where  $\mathcal{C}$  represents the conditional information pertinent to the corresponding  $X_1$ .

**Estimating Complex Spectrograms** Waveform reconstruction from complex spectrograms can be effectively achieved using the ISTFT. Notably, Vocos [12] and APNet2 [11], utilizing GANs as their model framework, estimate magnitude and phase spectrograms from the input Mel-spectrograms, which can be transformed to complex spectrograms effortlessly. Both models operate at the frame level, enabling them to achieve significantly faster inference speeds compared to HiFi-GAN [9], which uses multiple upsampling layers and operates at the level of waveform sample points. Moreover, these models preserve the quality of the synthesized waveform, demonstrating their superiority in both speed and fidelity without a trade-off. In this paper, we directly estimate complex spectrograms using Rectified Flow and focus on frame-level operations, aiming to enhance both the efficiency and quality of our waveform synthesis process. Notably, the distributions of real and imaginary parts of the complex spectrograms appear more homogeneous in comparison to the distributions magnitude and phase.

**Multi-band Audio Waveform Reconstruction** Both Multi-band MelGAN [24] and Multi-band Diffusion [21] employ multi-band strategies, albeit for different purposes within their respective frameworks. Multi-band MelGAN, specifically, uses Pseudo-Quadrature Mirror Filters (PQMF) [25] to divide frequency bands. This division results in each subband’s waveform being a fraction of the original waveform’s length, based on the number of subbands. By reshaping these subbands into feature dimensions and utilizing a unified backbone for modeling, Multi-band MelGAN is able to operate on considerably shorter signals. This strategy significantly enhances the efficiency of the model, leading to accelerated training and inference processes. Multi-band Diffusion utilizes an array of band-pass filters to separate the frequency bands and models each subband with a distinct model. This approach ensures that errors in one band do not negatively impact the others. In our research, we simplify the process of frequency band division by directly choosing the appropriate dimensions from the complex spectrograms. Furthermore, we enhance efficiency by modeling all subbands together in parallel with a single, unified model. This strategy improves the processing speed and also helps in reducing error accumulation across different subbands.

### 3 Method

Our model utilizes a multi-band Rectified Flow to directly predict the complex spectrogram. It operates at the STFT frame level and incorporates a highly efficient ConvNeXtV2 [23] backbone.

With only 10 steps of sampling, the model is capable of producing high-quality waveforms. In this section, we present the structure of the multi-band Rectified Flow model, which operates in either the time or frequency domain. We also describe its corresponding normalization techniques and three enhanced loss functions.

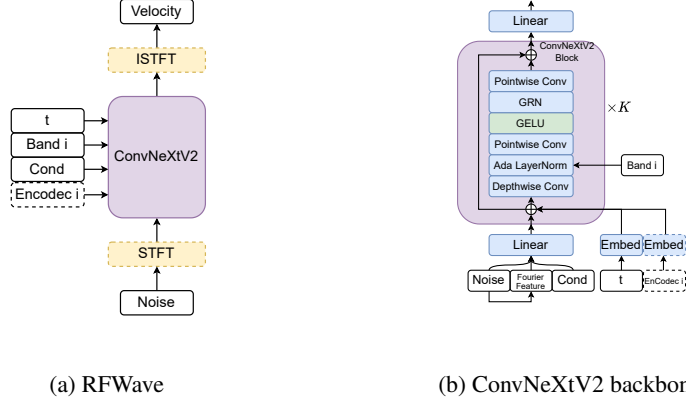


Figure 1: The overall structure for RFWave.  $\text{Band } i$  is the subband index,  $\text{Cond}$  is the conditional input, and  $\text{EnCodec } i$  is the EnCodec bandwidth index. Modules enclosed in a dashed box are considered optional.

### 3.1 Multi-band Rectified Flow

**Model Structure** The model structure is depicted in Figure 1a. All frequency bands, each distinguished by a unique subband index, share the same model. The subbands of a given sample are grouped together into a single batch for processing, which facilitates simultaneous training or inference. This significantly reduces inference latency. Moreover, independently modeling the subbands reduces error accumulation. As discussed in [21], conditioning higher bands on lower ones can lead to an error accumulation, which means inaccuracies in the lower bands can adversely affect the higher bands during inference.

For each subband, the corresponding noise is fed into the ConvNeXtV2 backbone to predict the velocity conditioned on time  $t$ , the subband index, conditional input (the Mel-spectrogram or the EnCodec [20] tokens), and an optional EnCodec bandwidth index. The detailed structure of the ConvNeXtV2 backbone is shown in Figure 1b. We employ Fourier features as described in [26]. The noise, Fourier features, and conditional inputs are concatenated and then passed through a linear layer, forming the input that is fed into a series of ConvNeXtV2 blocks. The sinusoidal time embedding, along with the optional EnCodec bandwidth index embedding, are element-wise added to the input of each ConvNeXtV2 block. Furthermore, the subband index is incorporated via an adaptive layer normalization module, which utilizes learnable embeddings as described in [12, 27]. The other components are identical to those within the ConvNeXtV2 architecture, details can be found in [23].

Our model, utilizing frame-level features, demonstrates greater memory efficiency compared to diffusion vocoders like PriorGrad that operate on waveform sample points. While PriorGrad [15] can train on 6-second<sup>1</sup> audio clips at 44.1 kHz within 30 GB of GPU memory, our model is capable of handling 177-second clips with the same memory resources.

**Operating in Time Domain and Waveform Equalization** Our model is designed to function at the STFT frame level and possesses the capability to operate in the time domain. Assuming that the noise and velocity reside in the time domain, the use of STFT and ISTFT, as illustrated in Figure 1a, becomes necessary. The dimensions of noise and velocity adhere to  $[1, T]$ , where  $T$  represents the waveform length in sample points<sup>2</sup>. After the STFT operation, we extract the subbands

<sup>1</sup>The duration of an audio clip is calculated as the batch size multiplied by the number of segment frames and hop length, divided by the sampling rate.

<sup>2</sup>For simplicity, the batch dimension is not included in the discussion.

by equally dividing the full-band complex spectrogram. Each subband  $i$  is then processed as an independent sample. Subsequently, these processed subbands are merged back together before the ISTFT operation. The feature processed by the backbone thus has dimensions of  $[d_s, F]$ , where  $d_s$  denotes the dimension of a subband’s complex spectrum and  $F$  the number of frames. The real and imaginary parts of each subband are interleaved to form a  $d_s$ -dimensional feature.

A white Gaussian noise signal has uniform energy distribution across all frequency bands. However, the energy profiles of various waveform types vary markedly among different frequency bands. For instance, the energy in a speech waveform exhibits an exponential decay with increasing frequency, whereas a music waveform tends to maintain a more consistent energy distribution across frequencies. These disparities pose challenges for training diffusion models. Consequently, it becomes advantageous to equalize the energy across waveform frequency bands [21]. In the time-domain model, a bank of Pseudo-Quadrature Mirror Filters (PQMF) is employed to decompose the input waveform into subbands. Subsequently, these subbands are equalized and then recombined to form the equalized waveform. The performance of the PQMF bank exhibits a modest enhancement compared to the array of band-pass filters employed in [21]. It’s important to note that the PQMF is solely utilized for waveform equalization and holds no association with the division of the complex spectrogram into subbands. For waveform equalization, mean-variance normalization is employed, utilizing the exponential moving average of mean and variance of each waveform subband computed during training. This approach ensures that the transformation can be effectively inverted using the same statistics.

**Alternative Approach: Operating in Frequency Domain and STFT Normalization** Assuming that noise and velocity reside in the frequency domain, the use of STFT and ISTFT, as depicted in Figure 1a, becomes unnecessary. The subbands of noise and velocity are then directly extracted from their full-band feature by selecting the corresponding dimensions, resulting in a shape of  $[d_s, F]$ . In the frequency-domain model, the waveform is transformed to a complex spectrogram without equalization. Subsequent processing involves the dimension-wise mean-variance normalization of the complex spectrogram.

During the inference stage, the model operating in the time domain requires two additional operations—STFT and ISTFT—at each sampling step. In contrast, the model operating in the frequency domain requires only a single ISTFT operation after sampling. However, despite the additional operations, the time-domain model demonstrates slightly superior performance, particularly in capturing high-frequency details according to our experiment results.

### 3.2 Loss functions

**Energy-balanced Loss** In our preliminary experiments, we observe the presence of low-volume noise in regions that are expected to be silent. We attribute this to the property of Mean Square Error (MSE) used in (2). The MSE measures the absolute distortion between the predicted values and the ground truth. Since the values in silent regions are close to zero, even a minor absolute distortion in predictions can lead to a significant relative error. Consequently, models trained with the MSE produce small absolute distortions in silent regions, which are then perceived as noise.

We propose energy-balanced loss to mitigate this problem. Our energy-balanced loss is designed to weight errors differently depending on the region’s volume (or energy) across the time-axis. Specifically, for each frequency subband, we compute the standard deviation along the feature dimension of the ground truth velocity to construct a weighting coefficient of size  $[1, F]$ . This vector is reflective of the frame-level energy of the respective subband, as depicted in Figure A.1. Subsequently, both the ground truth and predicted velocity are divided by this vector before proceeding to the subsequent steps. For the frequency domain model, the training objective defined in (2) is adjusted as follows:

$$\min_v \mathbb{E}_{X_0 \sim \pi_0, (X_1, \mathcal{C}) \sim D} \left[ \int_0^1 \| (X_1 - X_0)/\sigma - v(X_t, t | \mathcal{C})/\sigma \|^2 dt \right], \quad (5)$$

with  $\sigma = \sqrt{\text{Var}_1(X_1 - X_0)}$  and  $X_t = tX_1 + (1 - t)X_0$ ,

where  $D$  represents the dataset with paired  $X_1$  and  $\mathcal{C}$ , and  $\text{Var}_1$  calculates the variance along the feature dimension. For the time domain model, this energy balancing operation precedes the ISTFT

process. This approach helps to minimize the relative error in low-volume regions. Our experimental results demonstrate that this method enhances overall performance, benefiting not just the silent parts.

**Overlap Loss** Within the multi-band structure, each subband is predicted independently, potentially resulting in inconsistencies among them. To mitigate these inconsistencies, we introduce an overlap loss. This involves maintaining overlaps between the subbands when dividing the full-band complex spectrograms. A detailed illustration of this scheme is provided in Figure 2. The complex spectrogram is circularly padded in the feature dimension with a size of  $(d_{ol}, d_{ol} - 1)$ , where  $d_{ol}$  signifies the overlap size. The dimension of each subband’s main section, denoted as  $d_m$ , is calculated by dividing  $d - 1$  by the total number of subbands. Here,  $d$  represents the dimension of the complex spectrograms. The last subband is an exception, having an extra feature dimension but one less padding dimension. Subbands are extracted by applying a sliding window along the feature dimension, where the window has a size of  $d_m + 2d_{ol}$  and shifts by  $d_m$ <sup>3</sup>. In this paper, we employ an 8-dimensional overlap. During the training phase, the MSEs of the overlapped predictions is minimized. In the inference phase, the overlaps are removed, and all subbands are merged to recreate the full-band complex spectrograms. As each subband is predicted, the model internally maintains consistency between its overlap section and the main section. The overlap serves as an anchor to maintain consistency among the subbands.

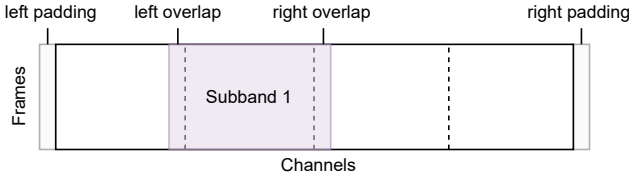


Figure 2: An illustration of dividing complex spectrograms into subbands. The area highlighted in purple represents a subband, while the section enclosed by the two dashed vertical lines indicates the main section.

**STFT Loss** The magnitude spectrogram derived loss [28] is extensively utilized in GAN-based vocoders, such as HiFi-GAN [9] and Vocos [12], both of which leverage a Mel-spectrogram loss. Nevertheless, its use in diffusion-based vocoders is relatively rare. This might stem from its lack of direct compatibility with the formalization of a noise prediction diffusion model. Here we adopt STFT loss for RFWave. According to (5), the model’s output serves as an approximation for velocity:

$$v(X_t, t | \mathcal{C}) \approx \frac{d}{dt} X_t = X_1 - X_0. \quad (6)$$

Hence, at time  $t$ , an approximation for  $X_1$  is:

$$\tilde{X}_1 \approx X_0 + v(X_t, t | \mathcal{C}). \quad (7)$$

The STFT loss can be applied on the approximation  $\tilde{X}_1$ , incorporating the spectral convergence loss and log-scale STFT-magnitude loss as proposed in [28]. According to our experimental findings, the STFT loss effectively reduces artifacts in the presence of background noise.

## 4 Experiments

**Overview** We evaluate our model across various auditory contexts, including singing (vocal), music (sound effects), and extensive speech datasets, validating its comprehensive applicability and efficiency in reconstructing audio waveforms from both Mel-spectrograms and discrete EnCodec tokens. Then, we conduct ablation studies to assess the impact of various design choices.

**Data** For waveform reconstruction from Mel-spectrograms, we use the Openccpop dataset [29] of 100 Mandarin songs for singing data, the MTG-Jamendo dataset [30] with over 55,000 tagged audio tracks for music, and the LibriTTS corpus[31], a multi-speaker English dataset with around 600 hours of diverse recordings, for speech data. When reconstructing waveforms from EnCodec

<sup>3</sup>The feature dimension of each subband, represented as  $d_s$ , equals  $2(d_m + 2d_{ol})$ , accounting for the interleave of real and imaginary parts.

tokens, we employ Common Voice 7.0 [32] and clean data from DNS Challenge 4 [33] for speech; the MTG-Jamendo dataset [30] for music; and FSD50K [34] and AudioSet [35] for environmental sounds.

For testing, we use 20 segments from Opencpop, a random selection of 300 sentences from the test-clean subset of LibriTTS, and 50 randomly selected audio files from MTG-Jamendo. When evaluating the quality of waveform reconstruction from Encodec tokens, we opt for an external dataset rather than a portion of the original. This more comprehensive and systematic approach covers as many domains and scenarios as possible. We have selected 900 test audio samples from 15 external datasets, spanning three major scenarios: speech, vocals, and sound effects. Details are provided in Table A.4.

**Implementation** We utilize the time-domain model with the 3 enhanced loss functions as the default configuration. The RFWave backbone contains 8 ConvNeXtV2 blocks, and the complex spectrogram is divided into 8 equally spanned subbands. For evaluation purposes, we use 10 sampling steps. Table A.3 lists the parameters used for extracting Mel-spectrograms and complex spectrograms from datasets with different sample rates. Additional details regarding the implementation can be found in the Appendix Section A.1. Information concerning the required computational resources is detailed in the Appendix Section A.2.

**Baseline and Evaluation Metrics** We conducted a comprehensive benchmark comparison of RFWave with several state-of-the-art methods, including Vocos [12], PriorGrad [15], and FreGrad [16], for reconstructing waveforms from Mel-spectrograms. Additionally, we compared RFWave with Multi-Band Diffusion (MBD) and the original EnCodec decoder for waveform reconstruction from Encodec tokens. For training Vocos, PriorGrad, and FreGrad, We adhered to the original training details provided by their open-sourced codes. The training was conducted separately on the LibriTTS, Opencpop, and MTG-Jamendo datasets, with the exception that a publicly available pre-trained Vocos model was utilized for the LibriTTS dataset. We also utilized publicly available pre-trained versions of MBD and EnCodec for comparison. We adhere to the sampling steps recommended by the authors for PriorGrad (6 steps), FreGrad (50 steps) and MBD (20 steps). The utilized repositories are detailed in Table A.2.

For the objective evaluation, we use ViSQOL [36] to assess perceptual quality, employing speech-mode for 22.05/24 kHz waveforms and audio-mode for 44.1 kHz waveforms. Additional metrics are also incorporated into our evaluation. Among these are the Perceptual Evaluation of Speech Quality (PESQ) [37], the F1 score for voiced/unvoiced classification (V/UV F1), and the periodicity error (Periodicity) [38]. As for the subjective evaluation, we conduct crowd-sourced assessments, employing a 5-point Mean Opinion Score (MOS) to determine the naturalness of the audio recordings. Participants are tasked with rating the speech samples on a scale from 1, denoting 'poor or completely unnatural', to 5, representing 'excellent or completely natural'.

## 5 Results

**Mel-spectrograms** The average MOS and objective metrics for various auditory contexts are listed in Table 1, and the separate results for each class are listed in Table A.5. RFWave outperforms the other models in most metrics. It achieves the highest scores in MOS, PESQ, and V/VU F1, and the lowest in periodicity error. Vocos achieves the highest ViSQOL, which might be misleading. In the MTG-Jamendo dataset, despite having the highest ViSQOL, Vocos exhibits a metallic artifacts that could affect the listening experience. This issue is also observed in [21] concerning GAN-based methods. The reason why RFWave obtains the best MOS may be because RFWave produces clearer and more consistent harmonics, especially in high-frequency. A collection of spectrograms and their corresponding analyses can be found in Appendix Section A.3.

**Discrete EnCodec Tokens** We use Classifier-Free Guidance (CFG) [39] with a coefficient of 2.0 for waveform reconstruction from EnCodec tokens, enhancing the listening experience significantly. However, its effect is less pronounced with waveform reconstruction from Mel-spectrograms, suggesting the ample, deterministic information in Mel-spectrograms reduces CFG's impact on the listening experience.

Table 1: Average Mean Opinion Score (MOS) and objective evaluation metrics for RFWave, Vocos, PriorGrad and FreGrad across various test sets. MOS is provided with 95% confidence interval

Model	MOS $\uparrow$	PESQ $\uparrow$	ViSQOL $\uparrow$	V/UV F1 $\uparrow$	Periodicity $\downarrow$
RFWave	<b>3.95</b> $\pm$ 0.09	<b>4.202</b>	4.456	<b>0.979</b>	<b>0.070</b>
Vocos	3.47 $\pm$ 0.10	3.530	<b>4.655</b>	0.973	0.088
PriorGrad	3.75 $\pm$ 0.09	3.612	4.347	0.974	0.082
FreGrad	2.99 $\pm$ 0.14	<u>3.640</u>	4.179	0.973	0.087
Ground truth	4.00 $\pm$ 0.09	-	-	-	-

Table 2 displays the average MOS and objective metrics for EnCodec tokens with varying bandwidths across different auditory contexts. Meanwhile, Table A.6 offers the individual results for each category. RFWave excels in all metrics, achieving optimal scores, except for ViSQOL. While using a larger bandwidth generally improves performance, for RFWave, an increase in bandwidth from 6.0 kbps to 12.0 kbps results in only a slight enhancement in MOS. Again, it is the EnCodec’s GAN-based decoder that attains the highest ViSQOL. This may indicate that different model families produce waveforms with different footprints. ViSQL appears to have a subtle bias towards the ones produced by the GAN-based model. MBD outperforms the original EnCodec decoder in subjective evaluations, a result that aligns with the findings reported in [21]. In Table A.6, it is evident that MBD performs particularly well in the sound effect dataset. This could be attributed to it having more parameters and being specifically designed for music generation.

Table 2: Average MOS and objective evaluation metrics for RFWave, EnCodec and MBD across various test sets.

Bandwidth	Model	MOS $\uparrow$	PESQ $\uparrow$	ViSQOL $\uparrow$	V/UV F1 $\uparrow$	Periodicity $\downarrow$
1.5 kbps	RFWave <sub>(CFG2)</sub>	<b>3.17</b> $\pm$ 0.22	<b>1.797</b>	3.108	<b>0.914</b>	<b>0.193</b>
	EnCodec	2.23 $\pm$ 0.23	1.708	<b>3.518</b>	0.906	0.199
	MBD	<u>3.01</u> $\pm$ 0.19	1.699	2.982	0.901	0.212
3.0 kbps	RFWave <sub>(CFG2)</sub>	<b>3.52</b> $\pm$ 0.25	<b>2.444</b>	3.570	<b>0.939</b>	<b>0.145</b>
	EnCodec	2.79 $\pm$ 0.25	1.934	<b>3.793</b>	0.930	0.166
	MBD	<u>3.06</u> $\pm$ 0.23	<u>2.310</u>	3.402	0.922	0.171
6.0 kbps	RFWave <sub>(CFG2)</sub>	<b>3.69</b> $\pm$ 0.16	<b>2.936</b>	3.892	<b>0.954</b>	<b>0.117</b>
	EnCodec	3.10 $\pm$ 0.15	2.432	<b>4.091</b>	0.951	0.126
	MBD	<u>3.43</u> $\pm$ 0.15	<u>2.488</u>	3.582	0.929	0.168
12.0 kbps	RFWave <sub>(CFG2)</sub>	<b>3.73</b> $\pm$ 0.16	<b>3.270</b>	<u>4.124</u>	<b>0.965</b>	<b>0.099</b>
	EnCodec	<u>3.55</u> $\pm$ 0.15	<u>2.892</u>	<b>4.291</b>	0.963	0.105
	MBD	-	-	-	-	-
Ground truth		4.07 $\pm$ 0.14	-	-	-	-

**Ablations** We perform ablation studies on the LJSpeech dataset [40], with 250 sentences reserved as a test set, specifically for waveform reconstruction from Mel-spectrograms. The performance metrics of the model, both in the frequency and time domains, with and without the implementation of the energy-balanced loss, are summarized in Table 3. Despite the metrics not consistently correlating with human evaluations, they accurately captured the quality improvements brought about by design modifications [21]. The model, operating in the time domain with the energy-balanced loss, demonstrates superior performance in terms of ViSQOL, V/UV F1, and periodicity error, outperforming the other three configurations. The overlap loss, STFT loss, and CFG are tested on this configuration. STFT loss improves PESQ scores but may negatively impact ViSQOL and periodicity error. This is due to the model’s tendency to prioritize magnitude over phase when STFT loss is applied. This trade-off is necessary to effectively remove artifacts, particularly when background noise is present. CFG consistently increases performance, however, it doubles the inference computation and increases latency by approximately 50%.



Table 3: Objective metrics assess the model’s performance in frequency (freq) and time (time) domains, with and without the inclusion of energy-balanced loss (energy-balanced), classifier-free guidance with a guidance coefficient of 2.0 (CFG2), overlap loss (overlap), and STFT loss (STFT).

Setting	PESQ $\uparrow$	ViSQOL $\uparrow$	V/UV F1 $\uparrow$	Periodicity $\downarrow$
freq w/o energy-balanced	3.872	4.430	0.948	0.144
freq w/ energy-balanced	3.901	4.433	0.950	0.140
time w/o energy-balanced	4.127	4.551	0.957	0.124
time w/ energy-balanced	4.181	4.598	0.965	0.110
w/ overlap	4.158	4.599	0.959	0.122
w/ overlap, STFT	4.211	4.578	0.961	0.119
w/ overlap, CFG2	4.225	4.671	<b>0.973</b>	<b>0.078</b>
w/ overlap, CFG2, STFT	<b>4.240</b>	4.663	0.972	0.081
Vocos <sub>(ISTFT)</sub>	3.787	<b>4.675</b>	0.961	0.108
PriorGrad	3.810	4.216	0.945	0.136
FreGrad	3.767	4.356	0.946	0.136

**Inference Speed** We perform inference speed benchmark tests using an NVIDIA GeForce RTX 4090 GPU. The implementation was done in PyTorch [41], and no specific hardware optimizations were applied. The inference was carried out with a batch size of 1 sample, utilizing the LJSpeech test set. Table 4 displays the synthesis speed and model size of the models. RFWave achieves the highest inference speed among the diffusion models, making latency no longer an obstacle for application. Vocos stands as a strong baseline given that it requires only a single forward pass and operates at the frame level.

Table 4: Model footprint and synthesis speed. xRT stands for the speed at which the model can generate speech in comparison to real-time. A higher xRT value signifies that the model is capable of producing speech quicker than real-time, with a value of 1.0 representing the speed of real-time.

Model	Parameters	GPU xRT( $\uparrow$ )	Sampling steps
RFWave	18.1 M	97.01	10
Vocos <sub>(ISTFT)</sub>	13.5 M	<b>2078.20</b>	1
PriorGrad	2.6 M	16.67	6
FreGrad	<b>1.7 M</b>	7.50	50
RFWave <sub>(CFG2)</sub>	18.1 M	64.87	10
MBD	411.0 M	4.82	20

## 6 Conclusion and Discussion

In this study, we propose RFWave, a multi-band Rectified Flow approach for audio waveform reconstruction. The model has been carefully designed to overcome the latency issues associated with diffusion models. RFWave stands out for its ability to generate complex spectrograms by operating at the frame level, processing all subbands concurrently. This concurrent processing significantly enhances the efficiency of the waveform reconstruction process. The empirical evaluations conducted in this research have demonstrated that RFWave achieves exceptional reconstruction quality. Moreover, it has shown superior computational efficiency by generating audio at a speed that is 97 times faster than real-time.

It would be relatively easy to implement the widely-used cascade pipeline to develop a Text-to-Speech (TTS) system. This involves mapping text features to Mel-spectrograms and then Mel-spectrograms to complex spectrograms using Rectified Flow for both stages. Nevertheless, it is more advantageous to map text features directly to complex spectrograms, especially in the context of rapidly evolving large-scale TTS models. Large-scale TTS models typically incorporate extensive corpora, and eliminating one stage of processing can significantly reduce computational resource requirements. Moreover, this direct approach minimizes the potential inconsistencies that may occur between the two stages. The infilling capabilities of Rectified Flow enable it to handle diverse functions similar to

those undertaken by prominent large-scale TTS models, for example, replicating the speaker’s voice and speech style from a provided audio prompt [42, 43]. We believe this approach warrants further investigation and plan to explore it in future work.

**Ethical Concerns** Our method, though not categorized as generative AI, is designed to be compatible with advanced techniques such as those in [17], improving the realism of synthesized speech. However, this also poses risks like the potential for creating convincing deepfakes and voice phishing scams.

## References

- [1] Hideki Kawahara, Ikuyo Masuda-Katsuse, and Alain De Cheveigne. Restructuring speech representations using a pitch-adaptive time–frequency smoothing and an instantaneous-frequency-based f0 extraction: Possible role of a repetitive structure in sounds. *Speech communication*, 27(3-4):187–207, 1999.
- [2] Masanori Morise, Fumiya Yokomori, and Kenji Ozawa. World: a vocoder-based high-quality speech synthesis system for real-time applications. *IEICE TRANSACTIONS on Information and Systems*, 99(7):1877–1884, 2016.
- [3] Aaron van den Oord, Sander Dieleman, Heiga Zen, Karen Simonyan, Oriol Vinyals, Alex Graves, Nal Kalchbrenner, Andrew Senior, and Koray Kavukcuoglu. Wavenet: A generative model for raw audio. *arXiv preprint arXiv:1609.03499*, 2016.
- [4] Nal Kalchbrenner, Erich Elsen, Karen Simonyan, Seb Noury, Norman Casagrande, Edward Lockhart, Florian Stimberg, Aaron Oord, Sander Dieleman, and Koray Kavukcuoglu. Efficient neural audio synthesis. In *International Conference on Machine Learning*, pages 2410–2419. PMLR, 2018.
- [5] Jean-Marc Valin and Jan Skoglund. Lpcnet: Improving neural speech synthesis through linear prediction. In *ICASSP 2019-2019 IEEE International Conference on Acoustics, Speech and Signal Processing (ICASSP)*, pages 5891–5895. IEEE, 2019.
- [6] Ian Goodfellow, Jean Pouget-Abadie, Mehdi Mirza, Bing Xu, David Warde-Farley, Sherjil Ozair, Aaron Courville, and Yoshua Bengio. Generative adversarial nets. In Z. Ghahramani, M. Welling, C. Cortes, N. Lawrence, and K.Q. Weinberger, editors, *Advances in Neural Information Processing Systems*, volume 27. Curran Associates, Inc., 2014.
- [7] Kundan Kumar, Rithesh Kumar, Thibault De Boissiere, Lucas Gestin, Wei Zhen Teoh, Jose Sotelo, Alexandre De Brebisson, Yoshua Bengio, and Aaron C Courville. Melgan: Generative adversarial networks for conditional waveform synthesis. *Advances in neural information processing systems*, 32, 2019.
- [8] Ryuichi Yamamoto, Eunwoo Song, and Jae-Min Kim. Parallel wavegan: A fast waveform generation model based on generative adversarial networks with multi-resolution spectrogram. In *ICASSP 2020-2020 IEEE International Conference on Acoustics, Speech and Signal Processing (ICASSP)*, pages 6199–6203. IEEE, 2020.
- [9] Jungil Kong, Jaehyeon Kim, and Jaekyoung Bae. Hifi-gan: Generative adversarial networks for efficient and high fidelity speech synthesis. *Advances in Neural Information Processing Systems*, 33:17022–17033, 2020.
- [10] Takuhiro Kaneko, Kou Tanaka, Hirokazu Kameoka, and Shogo Seki. istftnet: Fast and lightweight mel-spectrogram vocoder incorporating inverse short-time fourier transform. In *ICASSP 2022-2022 IEEE International Conference on Acoustics, Speech and Signal Processing (ICASSP)*, pages 6207–6211. IEEE, 2022.
- [11] Hui-Peng Du, Ye-Xin Lu, Yang Ai, and Zhen-Hua Ling. Apnet2: High-quality and high-efficiency neural vocoder with direct prediction of amplitude and phase spectra. *arXiv preprint arXiv:2311.11545*, 2023.
- [12] Hubert Siuzdak. Vocos: Closing the gap between time-domain and fourier-based neural vocoders for high-quality audio synthesis. *CoRR*, abs/2306.00814, 2023.
- [13] Zhifeng Kong, Wei Ping, Jiaji Huang, Kexin Zhao, and Bryan Catanzaro. Diffwave: A versatile diffusion model for audio synthesis. *arXiv preprint arXiv:2009.09761*, 2020.
- [14] Chris Donahue, Julian McAuley, and Miller Puckette. Adversarial audio synthesis. *arXiv preprint arXiv:1802.04208*, 2018.
- [15] Sang gil Lee, Heeseung Kim, Chaehun Shin, Xu Tan, Chang Liu, Qi Meng, Tao Qin, Wei Chen, Sungroh Yoon, and Tie-Yan Liu. Priorgrad: Improving conditional denoising diffusion models with data-dependent adaptive prior. In *International Conference on Learning Representations*, 2022.
- [16] Tan Dat Nguyen, Ji-Hoon Kim, Youngjoon Jang, Jaehun Kim, and Joon Son Chung. Fregrad: Lightweight and fast frequency-aware diffusion vocoder. In *International Conference on Acoustics, Speech, and Signal Processing (ICASSP)*, 2024.

- [17] Chengyi Wang, Sanyuan Chen, Yu Wu, Ziqiang Zhang, Long Zhou, Shujie Liu, Zhuo Chen, Yanqing Liu, Huaming Wang, Jinyu Li, et al. Neural codec language models are zero-shot text to speech synthesizers. *arXiv preprint arXiv:2301.02111*, 2023.
- [18] Dongchao Yang, Jinchuan Tian, Xu Tan, Rongjie Huang, Songxiang Liu, Xuankai Chang, Jiatong Shi, Sheng Zhao, Jiang Bian, Xixin Wu, et al. Uniaudio: An audio foundation model toward universal audio generation. *arXiv preprint arXiv:2310.00704*, 2023.
- [19] Neil Zeghidour, Alejandro Luebs, Ahmed Omran, Jan Skoglund, and Marco Tagliasacchi. Soundstream: An end-to-end neural audio codec. *IEEE/ACM Transactions on Audio, Speech, and Language Processing*, 30:495–507, 2021.
- [20] Alexandre Défossez, Jade Copet, Gabriel Synnaeve, and Yossi Adi. High fidelity neural audio compression. *CoRR*, abs/2210.13438, 2022.
- [21] Robin San Roman, Yossi Adi, Antoine Deleforge, Romain Serizel, Gabriel Synnaeve, and Alexandre Défossez. From discrete tokens to high-fidelity audio using multi-band diffusion. In *Thirty-seventh Conference on Neural Information Processing Systems*, 2023.
- [22] Xingchao Liu, Chengyue Gong, and Qiang Liu. Flow straight and fast: Learning to generate and transfer data with rectified flow. In *The Eleventh International Conference on Learning Representations, ICLR 2023, Kigali, Rwanda, May 1-5, 2023*. OpenReview.net, 2023.
- [23] Sanghyun Woo, Shoubhik Debnath, Ronghang Hu, Xinlei Chen, Zhuang Liu, In So Kweon, and Saining Xie. Convnext V2: co-designing and scaling convnets with masked autoencoders. In *IEEE/CVF Conference on Computer Vision and Pattern Recognition, CVPR 2023, Vancouver, BC, Canada, June 17-24, 2023*, pages 16133–16142. IEEE, 2023.
- [24] Geng Yang, Shan Yang, Kai Liu, Peng Fang, Wei Chen, and Lei Xie. Multi-band melgan: Faster waveform generation for high-quality text-to-speech. In *2021 IEEE Spoken Language Technology Workshop (SLT)*, pages 492–498, 2021.
- [25] J. Johnston. A filter family designed for use in quadrature mirror filter banks. In *ICASSP '80. IEEE International Conference on Acoustics, Speech, and Signal Processing*, volume 5, pages 291–294, 1980.
- [26] Diederik Kingma, Tim Salimans, Ben Poole, and Jonathan Ho. Variational diffusion models. In M. Ranzato, A. Beygelzimer, Y. Dauphin, P.S. Liang, and J. Wortman Vaughan, editors, *Advances in Neural Information Processing Systems*, volume 34, pages 21696–21707. Curran Associates, Inc., 2021.
- [27] Jingjing Xu, Xu Sun, Zhiyuan Zhang, Guangxiang Zhao, and Junyang Lin. Understanding and improving layer normalization. In H. Wallach, H. Larochelle, A. Beygelzimer, F. d'Alché-Buc, E. Fox, and R. Garnett, editors, *Advances in Neural Information Processing Systems*, volume 32. Curran Associates, Inc., 2019.
- [28] Sercan Arik, Heewoo Jun, and Gregory Diamos. Fast spectrogram inversion using multi-head convolutional neural networks. *IEEE Signal Processing Letters*, PP:1–1, 11 2018.
- [29] Yu Wang, Xinsheng Wang, Pengcheng Zhu, Jie Wu, Hanzhao Li, Heyang Xue, Yongmao Zhang, Lei Xie, and Mengxiao Bi. Openpop: A high-quality open source chinese popular song corpus for singing voice synthesis. In Hanseok Ko and John H. L. Hansen, editors, *Interspeech 2022, 23rd Annual Conference of the International Speech Communication Association, Incheon, Korea, 18-22 September 2022*, pages 4242–4246. ISCA, 2022.
- [30] Dmitry Bogdanov, Minz Won, Philip Tovstogan, Alastair Porter, and Xavier Serra. The mtg-jamendo dataset for automatic music tagging. In *Machine Learning for Music Discovery Workshop, International Conference on Machine Learning (ICML 2019)*, Long Beach, CA, United States, 2019.
- [31] Heiga Zen, Viet Dang, Rob Clark, Yu Zhang, Ron J Weiss, Ye Jia, Zhifeng Chen, and Yonghui Wu. Libritts: A corpus derived from librispeech for text-to-speech. *arXiv preprint arXiv:1904.02882*, 2019.
- [32] Rosana Ardila, Megan Branson, Kelly Davis, Michael Henretty, Michael Kohler, Josh Meyer, Reuben Morais, Lindsay Saunders, Francis M Tyers, and Gregor Weber. Common voice: A massively-multilingual speech corpus. *arXiv preprint arXiv:1912.06670*, 2019.

- [33] Harishchandra Dubey, Vishak Gopal, Ross Cutler, Ashkan Aazami, Sergiy Matuskevych, Sebastian Braun, Sefik Emre Eskimez, Manthan Thakker, Takuya Yoshioka, Hannes Gamper, and Robert Aichner. Icassp 2022 deep noise suppression challenge, 2022.
- [34] Eduardo Fonseca, Xavier Favory, Jordi Pons, Frederic Font, and Xavier Serra. Fsd50k: an open dataset of human-labeled sound events. *IEEE/ACM Transactions on Audio, Speech, and Language Processing*, 30:829–852, 2021.
- [35] Jort F Gemmeke, Daniel PW Ellis, Dylan Freedman, Aren Jansen, Wade Lawrence, R Channing Moore, Manoj Plakal, and Marvin Ritter. Audio set: An ontology and human-labeled dataset for audio events. In *2017 IEEE international conference on acoustics, speech and signal processing (ICASSP)*, pages 776–780. IEEE, 2017.
- [36] Michael Chinen, Felicia S. C. Lim, Jan Skoglund, Nikita Gureev, Feargus O’Gorman, and Andrew Hines. Visqol v3: An open source production ready objective speech and audio metric. In *2020 Twelfth International Conference on Quality of Multimedia Experience (QoMEX)*, pages 1–6, 2020.
- [37] A.W. Rix, J.G. Beerends, M.P. Hollier, and A.P. Hekstra. Perceptual evaluation of speech quality (pesq)-a new method for speech quality assessment of telephone networks and codecs. In *2001 IEEE International Conference on Acoustics, Speech, and Signal Processing. Proceedings (Cat. No.01CH37221)*, volume 2, pages 749–752 vol.2, 2001.
- [38] Max Morrison, Rithesh Kumar, Kundan Kumar, Prem Seetharaman, Aaron Courville, and Yoshua Bengio. Chunked autoregressive GAN for conditional waveform synthesis. In *International Conference on Learning Representations*, 2022.
- [39] Jonathan Ho and Tim Salimans. Classifier-free diffusion guidance. In *NeurIPS 2021 Workshop on Deep Generative Models and Downstream Applications*, 2021.
- [40] Keith Ito and Linda Johnson. The lj speech dataset. <https://keithito.com/LJ-Speech-Dataset/>, 2017.
- [41] Ian Goodfellow, Jean Pouget-Abadie, Mehdi Mirza, Bing Xu, David Warde-Farley, Sherjil Ozair, Aaron Courville, and Yoshua Bengio. Generative adversarial nets. In Z. Ghahramani, M. Welling, C. Cortes, N. Lawrence, and K.Q. Weinberger, editors, *Advances in Neural Information Processing Systems*, volume 27. Curran Associates, Inc., 2014.
- [42] Apoorv Vyas, Bowen Shi, Matthew Le, Andros Tjandra, Yi-Chiao Wu, Baishan Guo, Jiemin Zhang, Xinyue Zhang, Robert Adkins, William Ngan, Jeff Wang, Ivan Cruz, Bapi Akula, Akinniyi Akinyemi, Brian Ellis, Rashel Moritz, Yael Yungster, Alice Rakotoarison, Liang Tan, Chris Summers, Carleigh Wood, Joshua Lane, Mary Williamson, and Wei-Ning Hsu. Audiobox: Unified audio generation with natural language prompts, 2023.
- [43] Alexander H. Liu, Matthew Le, Apoorv Vyas, Bowen Shi, Andros Tjandra, and Wei-Ning Hsu. Generative pre-training for speech with flow matching. In *The Twelfth International Conference on Learning Representations*, 2024.
- [44] Tu Anh Nguyen, Wei-Ning Hsu, Antony d’Avirro, Bowen Shi, Itai Gat, Maryam Fazel-Zarani, Tal Remez, Jade Copet, Gabriel Synnaeve, Michael Hassid, et al. Espresso: A benchmark and analysis of discrete expressive speech resynthesis. *arXiv preprint arXiv:2308.05725*, 2023.
- [45] Evelina Bakhturina, Vitaly Lavrukhin, Boris Ginsburg, and Yang Zhang. Hi-fi multi-speaker english tts dataset. *arXiv preprint arXiv:2104.01497*, 2021.
- [46] Yao Shi, Hui Bu, Xin Xu, Shaoji Zhang, and Ming Li. Aishell-3: A multi-speaker mandarin tts corpus and the baselines. *arXiv preprint arXiv:2010.11567*, 2020.
- [47] Shinnosuke Takamichi, Kentaro Mitsui, Yuki Saito, Tomoki Koriyama, Naoko Tanji, and Hiroshi Saruwatari. Jvs corpus: free japanese multi-speaker voice corpus. *arXiv preprint arXiv:1908.06248*, 2019.
- [48] Frederico S Oliveira, Edresson Casanova, Arnaldo Candido Junior, Anderson S Soares, and Arlindo R Galvão Filho. Cml-tts: A multilingual dataset for speech synthesis in low-resource languages. In *International Conference on Text, Speech, and Dialogue*, pages 188–199. Springer, 2023.
- [49] Zafar Rafii, Antoine Liutkus, Fabian-Robert Stöter, Stylianos Ioannis Mimilakis, and Rachel Bittner. Musdb18-a corpus for music separation. 2017.

- [50] Soonbeom Choi, Wonil Kim, Saebyul Park, Sangeon Yong, and Juhan Nam. Children’s song dataset for singing voice research. In *International Society for Music Information Retrieval Conference (ISMIR)*, volume 4, 2020.
- [51] Dawn AA Black, Ma Li, and Mi Tian. Automatic identification of emotional cues in chinese opera singing. *ICMPC, Seoul, South Korea*, 2014.
- [52] Hiroki Tamaru, Shinnosuke Takamichi, Naoko Tanji, and Hiroshi Saruwatari. Jvs-music: Japanese multispeaker singing-voice corpus. *arXiv preprint arXiv:2001.07044*, 2020.
- [53] Steven R Livingstone and Frank A Russo. The ryerson audio-visual database of emotional speech and song (ravdess): A dynamic, multimodal set of facial and vocal expressions in north american english. *PloS one*, 13(5):e0196391, 2018.
- [54] Zhaorui Liu and Zijin Li. Music Data Sharing Platform for Computational Musicology Research (CCMUSIC DATASET), November 2021.
- [55] Karol J Piczak. Esc: Dataset for environmental sound classification. In *Proceedings of the 23rd ACM international conference on Multimedia*, pages 1015–1018, 2015.
- [56] Eric J. Humphrey, Simon Durand, and Brian McFee. Openmic-2018, September 2018.

## A Appendix

### A.1 Implementation Details

The RFWave backbone contains 8 ConvNeXtV2 blocks. Within each ConvNeXtV2 block, the depth-wise convolutional layer featuring a large kernel utilizes a kernel size of 7 and has a channel dimension of 512. The first and last 1x1 point-wise convolutional layers in the sequence possess channel dimensions of 512 and 1536, respectively.

During the extraction of complex coefficients for the model, we use the orthonormal Fast Fourier Transform (FFT) and its inverse (IFFT), with the normalization convention of dividing by  $1/\sqrt{N}$  for both operations, here  $N$  is the FFT size. This approach ensures the spectrogram extracted is within a more reasonable range for modeling.

In terms of loss functions, we assign a weight of 1 to either the Rectified Flow loss or its energy-balanced variant. If employed, the overlap loss and STFT loss are assigned a weight of 0.01. These weights are determined by aligning the L2-norm of the gradients from the overlap loss and STFT loss with approximately 1/10 of that from the Rectified Flow loss.

Training details are also worth mentioning. Audio samples are randomly cropped to lengths of 32512 and 65024 for 22.05/24 kHz and 44.1 kHz waveforms, respectively. This is equivalent to a crop window of 128 frames for both sampling rates. We use a batch size of 64. The model optimization is performed using the AdamW optimizer with a starting learning rate of  $2e-4$  and beta parameters of (0.9, 0.999). A cosine annealing schedule is applied to reduce the learning rate to a minimum of  $2e-6$ .

### A.2 Computational Resource Required for the Experiments

The bulk of the experiments were carried out on personal computers and GPU servers, which were sourced from cloud service providers. Primarily, we utilized Nvidia-4090-24G and Nvidia-A100-80G GPUs for these tasks.

The specific hardware used and the corresponding time taken for training RFWave on various datasets are as follows:

Table A.1: GPU configurations and training duration for various datasets

Dataset	GPU configuration	Training duration
LJspeech	1×4090	2 days
LibriTTS	2×A100	5 days
Opencpop	1×4090	1 day
MTG-Jamendo	2×A100	7 days
EnCodec Training	4×A100	10 days

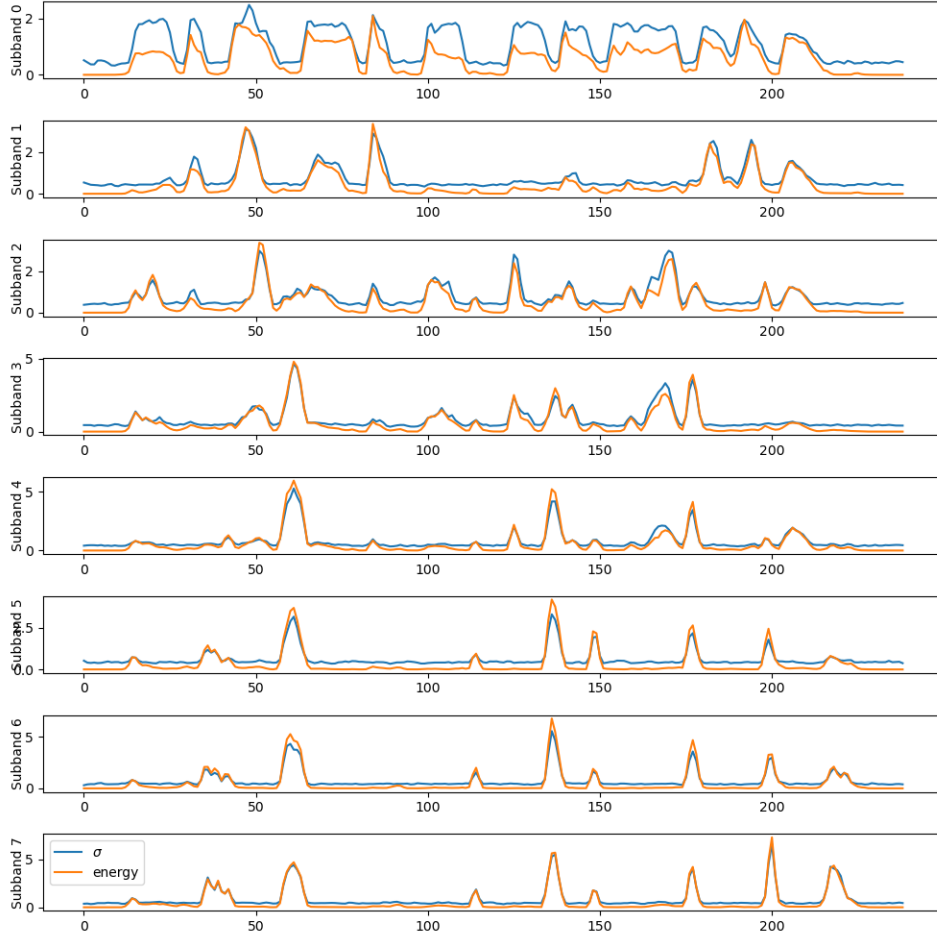


Figure A.1: The energy and weighting coefficients, represented by  $\sigma$ , display a consistent variation throughout the frames.

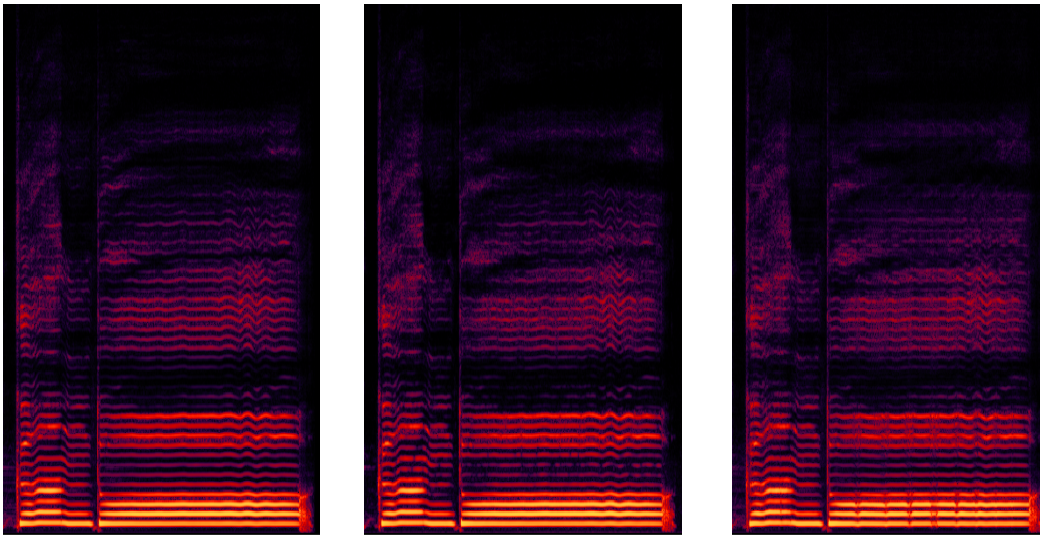
### A.3 Spectrogram Examples

Figure A.2 showcases spectrogram examples generated by various models using the Opencpop dataset. When compared to the ground truth spectrogram, RFWave is seen to produce clean and stable harmonics, whereas the harmonics generated by other models exhibit minor discontinuities.

Figure A.3 exhibits spectrogram examples generated by different models utilizing the LibriTTS dataset. RFWave and Vocos both generate clear high-frequency harmonics, while PriorGrad and FreGrad result in blurred high-frequency harmonics.

Figure A.4 displays spectrogram examples generated by diverse models from the Jamendo dataset. Both RFWave and PriorGrad generate commendable spectrograms, with RFWave edging out slightly in the high-frequency range. Interesting artifacts are observed in the spectrograms produced by Vocos and FreGrad. Vocos tends to generate very sharp and straight harmonics, leading to metallic sound. In contrast, FreGrad produces spectrograms with vertical lines, resulting in a sound that is jittery and discontinuous.

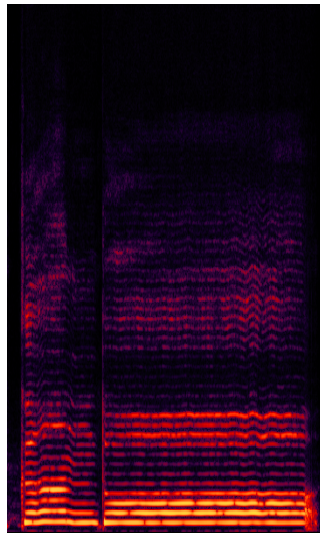




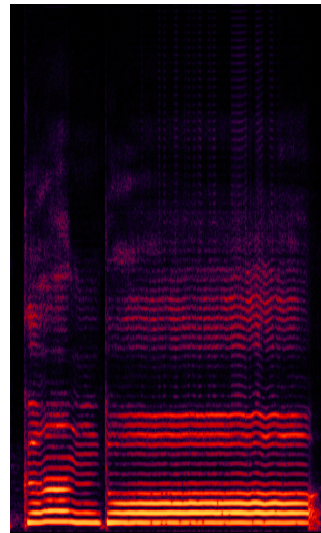
(a) Ground truth

(b) RFWave

(c) Vocos

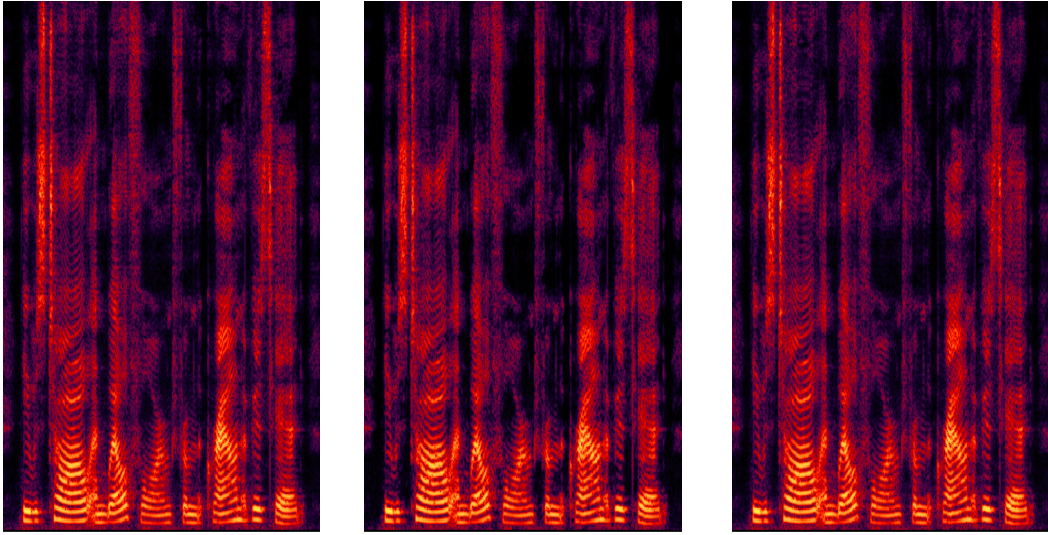


(d) PriorGrad



(e) FreGrad

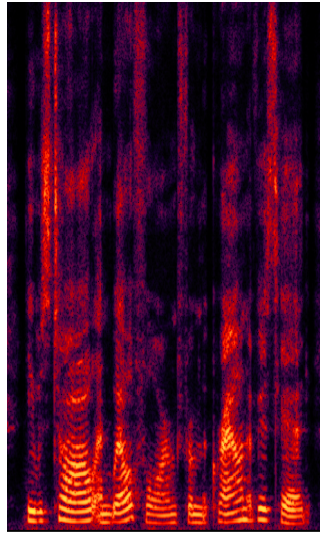
Figure A.2: Examples of spectrograms from Openpop



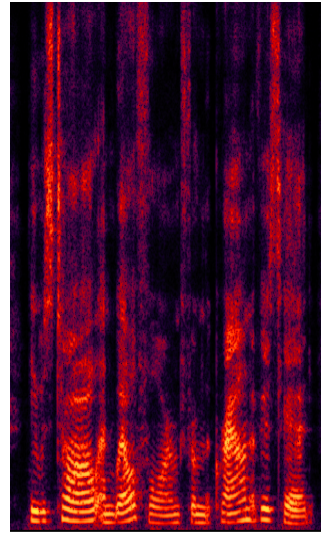
(a) Ground truth

(b) RFWave

(c) Vocos

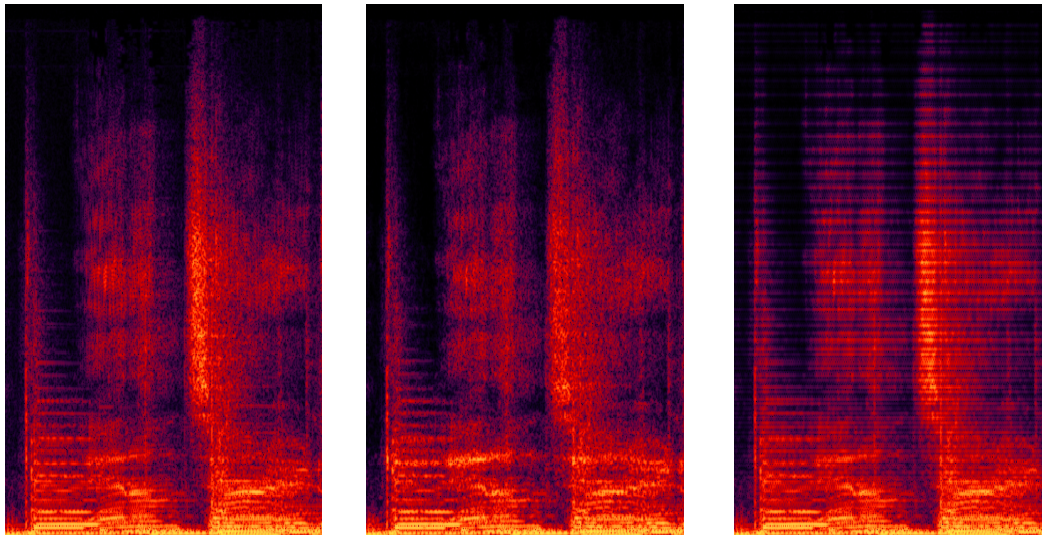


(d) PriorGrad



(e) FreGrad

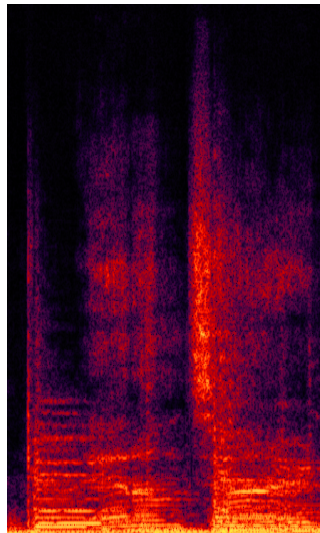
Figure A.3: Examples of spectrograms from LibriTTS



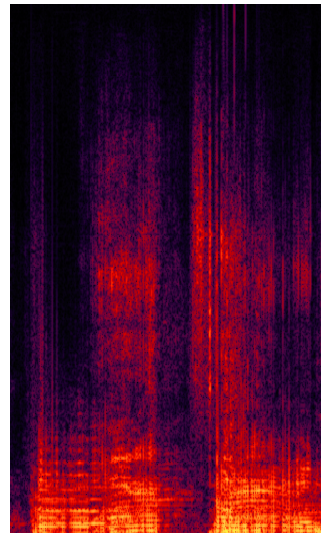
(a) Ground truth

(b) RFWave

(c) Vocos



(d) PriorGrad



(e) FreGrad

Figure A.4: Examples of spectrograms from MTG-Jamendo

## A.4 Tables

Table A.2: Code repositories for model training.

Model	repository
Vocos	<a href="https://github.com/gemelo-ai/vocos">https://github.com/gemelo-ai/vocos</a>
PriorGrad	<a href="https://github.com/microsoft/NeuralSpeech/tree/master/PriorGrad-vocoder">https://github.com/microsoft/NeuralSpeech/tree/master/PriorGrad-vocoder</a>
FreGrad	<a href="https://github.com/signofthefour/fregrad">https://github.com/signofthefour/fregrad</a>
Multi-Band Diffusion (MBD)	<a href="https://github.com/facebookresearch/audiocraft">https://github.com/facebookresearch/audiocraft</a>
EnCodec	<a href="https://github.com/facebookresearch/encodec">https://github.com/facebookresearch/encodec</a>

Table A.3: Parameters for extracting Mel-spectrograms and complex spectrograms.

Dataset	Sample rate (kHz)	Window length	Hop length	FFT size	Mel bins
LJSpeech	22.05	1024	256	1024	100
LibriTTS	24	1024	256	1024	100
Opencpop	44.1	2048	512	2048	100
MTG-Jamendo	44.1	2048	512	2048	100
EnCodec Training	24	1280	320	1280	-

Table A.4: Construction of the general Encodec test dataset

Category	Subdirectory	Samples	Description
Speech	Espresso-test	50	From the Espresso dataset test set [44], randomly select 50 samples, segmenting any audio longer than 30 seconds into 10-second clips beforehand.
	HiFiTTS-test	50	Randomly select 50 samples from the test set of the Hi-Fi TTS dataset [45].
	LibriTTS-test	50	Randomly select 50 samples from the test set of LibriTTS [31].
	Aishell3-test	50	Randomly select 50 samples from the test set of the Aishell3 dataset [46].
	JVS	50	Randomly select 50 samples from the entire JVS Corpus. [47].
	CML-TTS-test	50	Randomly select 50 samples from the test set of the CML-TTS dataset [48].
Vocal	Musdb-test-vocal	60	Segment the vocal track audio from the Musdb test set [49] into 10-second clips, then randomly select 60 samples.
	CSD	20	Segment all audio in the CSD [50] into 10-second clips, then randomly select 20 samples.
	Opencpop	20	Randomly select 20 samples from the Opencpop dataset [29].
	ChineseOpera-monophonic	60	From the monophonic subset of the Chinese Opera Singing Dataset [51], segment any audio longer than 30 seconds into 10-second clips, then randomly select 60 samples.
	JVS-Music	60	Randomly select 60 samples from the JVS-Music Corpus [52].
	RAVDESS	60	Randomly select 60 samples from the song subset of the RAVDESS corpus [53].
	Ccmusic-demo-vocal	20	From the demo audios of the Ccmusic Dataset [54], select the vocal parts. Then, randomly select 20 samples from these for the test set, segmenting any audio longer than 30 seconds into 10-second clips beforehand.
Sound Effect	ESC-50	150	Randomly select 150 samples from the ESC-50 [55].
	Musdb-test-accompaniment	40	Segment the accompaniment track audio from the test set of the Musdb dataset [49] into 10-second clips, then randomly select 40 samples from these clips.
	Musdb-test-mixture	20	Segment the mixture track audio from the test set of the Musdb dataset [49] into 10-second clips, then randomly select 20 samples from these clips.
	ChineseOpera-polyphonic	20	From the polyphonic subset of the Chinese Opera Singing Dataset [51], segment any audio longer than 30 seconds into 10-second clips, then randomly select 20 samples.
	OpenMIC-test	40	Randomly select 40 samples from the test set of OpenMix 2018 [56].
	Ccmusic-demo-music	30	From the demo audios of the Ccmusic Dataset [54], select the non-vocal parts. Then, randomly select 20 samples from these for the test set, segmenting any audio longer than 30 seconds into 10-second clips beforehand.

Table A.5: MOS and Objective evaluation metrics for RFWave, Vocos, PriroGrad and FreGrad across various datasets.

Dataset	Model	MOS $\uparrow$	PESQ $\uparrow$	ViSQOL $\uparrow$	V/UV F1 $\uparrow$	Periodicity $\downarrow$
LibriTTS	RFWave	$3.83 \pm 0.14$	4.228	4.595	0.968	0.090
	Vocos	$3.85 \pm 0.14$	3.660	4.696	0.958	0.104
	PriroGrad	$3.70 \pm 0.16$	3.820	4.134	0.960	0.100
	FreGrad	$3.68 \pm 0.15$	3.758	4.278	0.960	0.099
	Ground truth	$3.88 \pm 0.15$	-	-	-	-
Opencpop	RFWave	$4.26 \pm 0.17$	4.176	4.564	0.990	0.049
	Vocos	$3.84 \pm 0.19$	3.400	4.644	0.987	0.071
	PriroGrad	$3.79 \pm 0.21$	3.404	4.512	0.988	0.064
	FreGrad	$3.73 \pm 0.20$	3.522	4.507	0.986	0.074
	Ground truth	$4.33 \pm 0.18$	-	-	-	-
MTG-Jamendo	RFWave	$3.90 \pm 0.15$	-	4.317	-	-
	Vocos	$2.87 \pm 0.16$	-	4.628	-	-
	PriroGrad	$3.79 \pm 0.14$	-	4.412	-	-
	FreGrad	$1.89 \pm 0.17$	-	3.765	-	-
	Ground truth	$3.93 \pm 0.15$	-	-	-	-

Table A.6: MOS and objective evaluation metrics for RFWave, EnCodec and MBD across various test sets.

Test set	Bandwidth	Model	MOS	PESQ $\uparrow$	ViSQOL $\uparrow$	V/UV F1 $\uparrow$	Periodicity $\downarrow$	
Speech	1.5 kbps	RFWave <sub>(CFG2)</sub>	3.29 $\pm$ 0.47	1.774	3.102	0.913	0.178	
		EnCodec	2.29 $\pm$ 0.35	1.515	3.310	0.870	0.231	
		MBD	2.94 $\pm$ 0.29	1.659	2.793	0.901	0.195	
	3.0 kbps	RFWave <sub>(CFG2)</sub>	3.85 $\pm$ 0.39	2.421	3.582	0.935	0.137	
		EnCodec	2.85 $\pm$ 0.47	1.967	3.746	0.919	0.166	
		MBD	2.88 $\pm$ 0.33	2.194	3.219	0.915	0.166	
	6.0 kbps	RFWave <sub>(CFG2)</sub>	4.05 $\pm$ 0.26	2.974	3.913	0.952	0.109	
		EnCodec	3.19 $\pm$ 0.31	2.554	4.048	0.945	0.121	
		MBD	3.51 $\pm$ 0.30	2.372	3.410	0.924	0.161	
	12.0 kbps	RFWave <sub>(CFG2)</sub>	3.96 $\pm$ 0.22	3.393	4.158	0.965	0.089	
		EnCodec	3.52 $\pm$ 0.22	3.104	4.250	0.961	0.095	
		MBD	-	-	-	-	-	
		Ground truth		4.13 $\pm$ 0.23	-	-	-	-
	Vocal	1.5 kbps	RFWave <sub>(CFG2)</sub>	3.06 $\pm$ 0.34	1.820	3.317	0.914	0.208
			EnCodec	1.94 $\pm$ 0.38	1.900	3.931	0.941	0.166
MBD			2.84 $\pm$ 0.31	1.739	3.221	0.901	0.228	
3.0 kbps		RFWave <sub>(CFG2)</sub>	3.47 $\pm$ 0.34	2.467	3.793	0.942	0.152	
		EnCodec	2.63 $\pm$ 0.37	1.900	3.931	0.941	0.166	
		MBD	3.26 $\pm$ 0.45	2.426	3.655	0.929	0.175	
6.0 kbps		RFWave <sub>(CFG2)</sub>	3.77 $\pm$ 0.23	2.897	4.080	0.956	0.124	
		EnCodec	2.92 $\pm$ 0.23	2.310	4.206	0.956	0.131	
		MBD	3.30 $\pm$ 0.26	2.604	3.840	0.933	0.175	
12.0 kbps		RFWave <sub>(CFG2)</sub>	3.83 $\pm$ 0.31	3.147	4.273	0.964	0.109	
		EnCodec	3.40 $\pm$ 0.29	2.679	4.373	0.965	0.114	
		MBD	-	-	-	-	-	
		Ground truth		4.27 $\pm$ 0.24	-	-	-	-
Sound Effect		1.5 kbps	RFWave <sub>(CFG2)</sub>	3.24 $\pm$ 0.43	-	2.906	-	-
			EnCodec	2.62 $\pm$ 0.42	-	3.314	-	-
	MBD		3.33 $\pm$ 0.36	-	2.932	-	-	
	3.0 kbps	RFWave <sub>(CFG2)</sub>	3.11 $\pm$ 0.59	-	3.334	-	-	
		EnCodec	2.89 $\pm$ 0.48	-	3.703	-	-	
		MBD	3.11 $\pm$ 0.54	-	3.331	-	-	
	6.0 kbps	RFWave <sub>(CFG2)</sub>	3.27 $\pm$ 0.27	-	3.682	-	-	
		EnCodec	3.17 $\pm$ 0.24	-	4.020	-	-	
		MBD	3.44 $\pm$ 0.23	-	3.496	-	-	
	12.0 kbps	RFWave <sub>(CFG2)</sub>	3.33 $\pm$ 0.28	-	3.942	-	-	
		EnCodec	3.72 $\pm$ 0.26	-	4.249	-	-	
		MBD	-	-	-	-	-	
		Ground truth		3.78 $\pm$ 0.28	-	-	-	-